Phase transition and defects in a thin nematic film

Y. Lansac and F. Fried
Laboratoire de Physique de la Matière Condensée, URA 190, Parc Valrose, 06108 Nice Cedex 2, France

P. Maïssa
Institut Non Linéaire de Nice, UMR 129, 1361 route des Lucioles, 06560 Valbonne, France
(Received 24 October 1994)

We derive a set of general equations of the Landau-Ginzburg type describing the spatiotemporal evolutions of the tensorial order parameter of the nematic phase. We study numerically, for a particular case (thin nematic film), the equilibrium points and the dynamical behavior (pattern formation, nucleation and growth processes, and defects) of the isotropic-anisotropic phase transition. We discuss the biaxial zones, which are located at the core of the defects and at the interfaces of the nucleating domains, and the shape of these nuclei.

PACS number(s): 61.30.Jf, 64.70.Md, 05.70.Fh, 47.20.Hw

I. INTRODUCTION

The isotropic-anisotropic nematic phase transition has been extensively studied from both experimental and theoretical points of view during the past twenty years [1]. When a nematic liquid crystal is quenched from a high-temperature phase, where it is in a homogeneous isotropic stable state, to a lower-temperature phase, where this state becomes metastable with respect to an anisotropic one, a first-order phase transition takes place [2]. The time evolution of the system is governed by a nucleation and growth process and since the molecular orientations are random inside the nematic phase, by domain coalescence, a great number of topological defects appear. The number density of these defects decreases as a function of time, leading the sample towards a homogeneous anisotropic phase, without defect. With the help of a set of nonlinear partial derivative equations describing the spatiotemporal evolutions of the tensorial order parameter Q_{ij} [3,4], we study the dynamics of the isotropic-nematic phase transition (nucleation and growth) and the time evolution law of defects in the anisotropic phase [5] of a thin nematic film.

These problems are of real technological interest since they govern the mechanical properties of these materials. We particularly analyze the influence of the elastic constant values on both the nucleating domain growth and the director field at the isotropic-anisotropic interfaces.

II. MODEL

A. Order parameter

The isotropic-anisotropic phase transition is described by a continuum theory. In this case, we focus our attention on a small set of semimacroscopic variables whose dynamical evolutions are "slow" compared to the remaining degrees of freedom. The dynamical equations of motions for this set of variables are then obtained by either phenomenological arguments [4] or formal projection operator techniques [6]. The choice of the variables is very important; we do not want to omit any essential features or introduce any unnecessary complexity.

The difference between the orientational order properties of the high-temperature isotropic liquid and the low-temperature nematic mesophase is revealed by the measurement of all the macroscopic tensor properties such as the magnetic and dielectric susceptibilities or the refractive indices [3]. Then the convenient order parameter, defined at the lower expansion order and taking into account both the preferred directions of the molecules (directors) and the degree of order around these directions (orientational order parameters), is a symmetric second-rank tensor, which describes the head-tail symmetry of the nematic phase. These preferred directions are identified by unit vectors, so the order parameter verifies $\mathrm{Tr}Q=0$.

In the equilibrium anisotropic state or far from the defect zones, the nematic liquid crystal is homogeneous and uniaxial and then described by a tensorial order parameter $Q_{ij}=S/2(3n_in_j-\delta_{ij})$, where n_i are the director components and S is the conventional scalar orientational order parameter. However, in the defects zones or at the isotropic-anisotropic interface, a full description taking into account the biaxiality of the system must be considered [7].

B. Free energy density

The phenomenological free energy density f derived by de Gennes upon symmetry arguments is constituted by two parts: a homogeneous one (the bulk free energy density) and an inhomogeneous one (the gradient free energy density) describing the spatial variations of the tensorial order parameter (coarse grained approximation). Since the transition is weakly first order, the free energy density can be expanded around the isotropic phase of the nematic liquid crystal. The expansion is made at high enough order to ensure the thermodynamical stability of the system. For this reason and keeping in mind that the free

 ©1995 The American Physical Society

energy must be a scalar quantity, one only retains the terms up to fourth order for the bulk free energy density and to second order for the gradient energy density; these last terms are taken to be only quadratic in Q_{ij} [8]:

$$f \propto \frac{a}{2}(T-T^*)Q_{ij}(\mathbf{r})Q_{ij}(\mathbf{r})+\frac{b}{3}Q_{ij}(\mathbf{r})Q_{jk}(\mathbf{r})Q_{ki}(\mathbf{r}) + \frac{c_1}{4}[Q_{ij}(\mathbf{r})Q_{ji}(\mathbf{r})]^2+\frac{c_2}{4}Q_{ij}(\mathbf{r})Q_{jk}(\mathbf{r})Q_{kl}(\mathbf{r})Q_{li}(\mathbf{r}) + \frac{L_1}{2}[\partial_i Q_{jk}(\mathbf{r})]^2+\frac{L_2}{2}\partial_i Q_{ij}(\mathbf{r})\partial_k Q_{kj}(\mathbf{r}) , \quad (1)$$

where $i,j,k=x,y,z$; a,b,c_1,c_2 are temperature-dependent coefficients derived from a mean-field-type theory [9], and L_1,L_2 are phenomenological coefficients related to the nematic elastic constants. T^* is the temperature of the limit of stability of the isotropic phase.

We also define the temperature T^{**}, above which only the isotropic phase exists, and the isotropic-anisotropic transition temperature T_c (Fig. 1). For small molecules liquid crystal and in our model (mean-field theory), we have $T^*/T_c=0.863$ and $T^{**}/T_c=1.017$. Then, the range of temperature $[T^*,T^{**}]$ represents the metastability zone into which a coexistence between the isotropic and nematic phases is possible. We must note that this coexistence is an equilibrium state, only at T_c (isotropic-anisotropic phase equiprobability). Below T_c, the anisotropic phase expands with time to the detriment of the isotropic phase and above T_c the situation is reversed.

The free energy density [Eq. (1)] allows the full description of both the phase transition phenomena (nucleation and growth process) and the defect behavior in the anisotropic phase. It contains, in addition to the classical term describing the homogeneous free energy density (Landau–de Gennes expansion), terms accounting for the spatial variations of $S(\mathbf{r})$ and $\hat{\mathbf{n}}(\mathbf{r})$ and coupling terms between them, with the surface contribution being omitted.

We recover two particular limit cases. The first case corresponds to a fixed uniform director field and allows the description of the phase transition by scalar order parameters. In an uniaxial phase, we have, from Eq. (1),

$$f \propto AS^2-BS^3+CS^4+\frac{3}{4}\left[L_1+\frac{L_2}{6}\right](\nabla S)^2 + \frac{3}{8}L_2(\hat{\mathbf{n}}\cdot\nabla S)^2 , \quad (2)$$

where A, B, and C are related respectively, to a, b, and c_1,c_2. The second case corresponds to an anisotropic medium in which the orientational parameter is spatially invariant (Frank elastic free energy [10]).

In the uniaxial limit, the elastic deformations of a nematic phase are described, from Eq. (1), by

$$f \propto \left[L_1+\frac{L_2}{2}\right](\nabla\cdot\hat{\mathbf{n}})^2+L_1(\hat{\mathbf{n}}\cdot\nabla\times\hat{\mathbf{n}})^2 + \left[L_1+\frac{L_2}{2}\right](\hat{\mathbf{n}}\times\nabla\times\hat{\mathbf{n}})^2 . \quad (3)$$

The three coefficients introduced in this expression are related, respectively, to the splay $K_{11}\propto(L_1+L_2/2)$, twist $K_{22}\propto L_1$, and bend $K_{33}\propto(L_1+L_2/2)$ elastic coefficients, defined by Frank. We must note that, at this order of expansion of the Landau–de Gennes free energy density, there are only two independent elastic constants, with the bend and splay coefficients always being equal [8]. Then we define an elasticity anisotropy parameter K

$$K=(L_2/2)/(L_1+L_2/2)=1-K_{22}/K_{11} , \quad (4)$$

which represents the anisotropic character of the dynamical process and is equal to zero, in the uniaxial limit, when all three elastic constants are equal.

Through several experimental determinations of the elastic constants, we have estimated the mean value of the K parameter, introduced in our phenomenological model, to 0.4. Indeed, for model liquid crystals 4-methoxybenzylidene-4′-*n*-butylaniline (MBBA), O-hydroxy-*p*-methoxybenzylidene-*p*′-butylaniline (OHMBBA), 4′-*n*-pentyl-4-cyanobiphenyl (5CB), and para-azoxyanisole (PAA), K is equal, respectively, to 0.39 (at $T/T_c=0.96$) [11], 0.37 (at $T/T_c=0.98$) [11], 0.48 (at $T/T_c=0.98$) [12], and 0.36 (at $T/T_c=0.97$) [13,14].

We must note that the validity of the two elastic constant approximation is more questionable. It is only verified for a small number of molecules, for example, MBBA ($K_{33}/K_{11}=1.06$ at $T/T_c=0.96$ [11]) or OHMBBA ($K_{33}/K_{11}=1.06$ at $T/T_c=0.98$ [11]), or very near the transition temperature, for example, for PAA, where K_{33}/K_{11} is equal, respectively, to 2.1 at $T/T_c=0.97$ and to 1.7 at $T/T_c\approx 1$ [14].

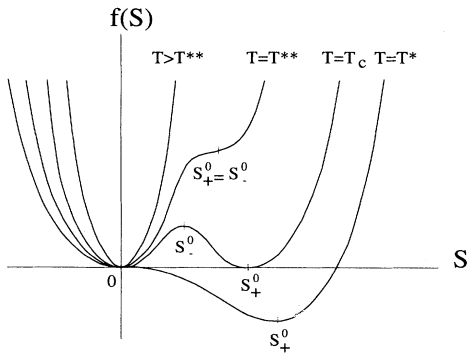

FIG. 1. Shape of the free energy density of Landau–de Gennes type as a function of temperature. In our model, $T^*/T_c=0.863$ and $T^{**}/T_c=1.017$. For the reduced temperature T^*/T_c, we have $S^0_-=0$. S^0_+ and S^0_- correspond to stable, metastable, or unstable states, as explained in Sec. III C and Appendix B.

C. Dynamical phenomenological equations

We assume that the spatiotemporal evolution of the tensorial order parameter $Q_{ij}(\mathbf{r},t)$ is governed by the variations of the free energy $\mathcal{F}$ (variational problem) [2,15]. Then, we write a Ginzburg-Landau-type equation for the nonconservative order parameter Q_{ij}:

$$\frac{dQ_{ij}}{dt}=-M_{ij}\frac{\delta\mathcal{F}}{\delta Q_{ij}}\ , \tag{5}$$

with $i,j=1,2,3$; $\mathcal{F}=\int f(Q)d\mathbf{r}$; and M_{ij}, the rotational kinetic coefficients, taken as $M_{11}=M_{22}=M_{33}=2M_{13}=2M_{23}=M$.

In general (phase transition and defects in a three-dimensional thermotropic nematic), we have, with the constraints $\mathrm{Tr}Q=0$ and $Q_{ij}=Q_{ji}$, a set of five coupled nonlinear partial derivative equations describing the spatiotemporal evolutions of the tensor components Q_{11}, Q_{22}, Q_{12}, Q_{13}, and Q_{23}. We rewrite the nonlinear dynamical equations [Eq. (4)] in a more convenient form by introducing a scalar quantity Q_S and two complex quantities Q_1 and Q_2 defined by

$$Q_1=Q_{1R}+iQ_{1I}\ ,\quad Q_2=Q_{2R}+iQ_{2I}\ . \tag{6}$$

We make the following change of variables:

$$\begin{aligned}
&Q_S=Q_{11}+Q_{22}\ ,\\
&Q_{1R}=Q_{11}-Q_{22}\ ,\\
&Q_{1I}=2Q_{12}\ ,\\
&Q_{2R}=2Q_{13}\ ,\\
&Q_{2I}=2Q_{23}\ .
\end{aligned} \tag{7}$$

Then, in the special case of a uniaxial nematic phase, Q_S, Q_{1R}, and Q_{1I} are expressed as functions of the director components $n_1=\sin\theta\cos\varphi$, $n_2=\sin\theta\sin\varphi$, and $n_3=\cos\theta$ (where θ is the polar angle and φ the azimuthal one),

$$\begin{aligned}
&Q_S=\frac{S}{2}(3\sin^2\theta-2)\ ,\\
&Q_{1R}=\frac{3S}{2}\sin^2\theta\cos2\varphi\ ,\\
&Q_{1I}=\frac{3S}{2}\sin^2\theta\sin2\varphi\ ,\\
&Q_{2R}=\frac{3S}{2}\sin2\theta\cos\varphi\ ,\\
&Q_{2I}=\frac{3S}{2}\sin2\theta\sin\varphi\ .
\end{aligned} \tag{8}$$

Finally, we also rescale time and space ($t\rightarrow\bar{t}/M$ and $x\rightarrow\bar{x}\sqrt{L_1+L_2/2}$), where $\bar{t}$ and $\bar{x}$ are dimensionless variables. Then the full set of equations is rewritten in the form given in Appendix A.

III. THIN NEMATIC FILM

A. Evolution equations

The general set of equations of evolution is considerably simplified in some particular cases. In the following, we consider a three-dimensional system with an anchoring energy on the glasses, which allows an orientation of the local directors either parallel ("planar degenerate" case) or perpendicular (homeotropic case) to the surfaces. This anchoring is described by a quadratic contribution in the components of the tensorial order parameter to the free energy density [16]. Moreover, it is taken sufficiently weak to ensure a first-order phase transition towards a uniaxial nematic phase [16]. In addition, we neglect the spatial variations of the order parameter in the z direction; so the thickness of the film must be much smaller than the other two dimensions. We have not explicitly introduced the anchoring quadratic term into the model; due to these assumptions, this term would only slightly modify the numerical values of the temperatures of the limit of metastability and of the transition, which are already phenomenological quantities.

Under these assumptions, we have $\partial_3 Q_i=0$ for any $i=S,1R,1I$ and $Q_2=0$. Then the set of five equations is reduced to two, which are rewritten

$$\begin{aligned}
\frac{dQ_S}{dt}=-3\Big\{&\frac{B}{2}|Q_1|^2+2(A+C|Q_1|^2)Q_S\\
&-\frac{3B}{2}Q_S^2+6CQ_S^3-\left[1-\frac{2}{3}K\right]\nabla^2Q_S\\
&-\frac{K}{6}(\partial_{\chi\chi}\bar{Q}_1+\partial_{\bar{\chi}\bar{\chi}}Q_1)\Big\}\ ,
\end{aligned} \tag{9}$$

$$\begin{aligned}
\frac{dQ_1}{dt}=-\{&(2A+3BQ_S+6CQ_S^2)Q_1+2C|Q_1|^2Q_1\\
&-\nabla^2Q_1-K\partial_{\chi\chi}Q_S\}\ ,
\end{aligned} \tag{10}$$

where $\bar{Q}_1$ is the conjugated complex of Q_1 and $|Q_1|^2=Q_{1R}^2+Q_{1I}^2$. The operator ∂_χ is defined as $\partial_\chi=\partial_1+i\partial_2$; then we have $\partial_{\chi\chi}=\partial_1^2-\partial_2^2+2i\partial_1\partial_2$ and $\partial_{\bar{\chi}\bar{\chi}}=\partial_1^2-\partial_2^2-2i\partial_1\partial_2$. In addition to a scalar equation, we have a complex equation that is very similar to the usual Ginzburg-Landau equation (plus an anisotropic term K).

B. Equations resolution and order parameters visualization

The set of nonlinear partial derivative equations are numerically solved by using an explicit finite difference scheme (first-order right difference scheme for time and fourth-order centered difference scheme for space) on a square grid of 128×128 pixels, on a highly parallel computer (Connection Machine CM-200). These simulations are interactive: real-time variations of the parameters governing the evolution of the system.

The visualization in physical space (directors and orientational order parameters) is obtained at a given time by diagonalization of the tensor Q_{ij}; the directors are given by the eigenvectors and the orientational order parameters by the associated eigenvalues. In the case of a thin nematic film, as previously defined, we always have one of the eigenvectors perpendicular to the plane into which the molecules lie, the two others being in the plane itself. Then we arbitrarily choose one of these last two eigenvectors to represent one of the preferred directions of the molecules, the other (in the case when its exists, then in the biaxiality zones) being given by the other eigenvector.

The orientational order parameters describing the iso-

tropic zones and uniaxial or biaxial anisotropic zones correspond, respectively, to three zero eigenvalues and two equal or three different nonzero eigenvalues. We must also note that, since the order parameter is a tensor, the defects observed in the space (Q_1, Q_S) have strengths equal to twice those observed in the real physical space.

C. Associated dynamical system

The dynamical system, associated with our set of spatiotemporal evolution equations, is deduced from Eqs. (9) and (10):

$$\frac{dQ_S}{dt} = -3\left\{\frac{B}{2}|Q_1|^2 + 2(A + C|Q_1|^2)Q_S - \frac{3B}{2}Q_S^2 + 6CQ_S^3\right\}, \tag{11}$$

$$\frac{dQ_1}{dt} = -\{(2A + 3BQ_S + 6CQ_S^2)Q_1 + 2C|Q_1|^2 Q_1\}. \tag{12}$$

We consider the fixed points of this system, which represent the equilibrium or stationary states of the nematic liquid crystal. Then they satisfy the identity $dQ_S/dt = dQ_1/dt = 0$.

We find five fixed points (Figs. 2 and 3). They can be regrouped into three sets, which obey

$$Q_S = Q_1 = 0; \tag{13}$$

$$|Q_1| = 0, \quad Q^0_{S_\pm} = \frac{B}{8C}\left[1 \pm \left[1 - \frac{64AC}{3B^2}\right]^{1/2}\right]; \tag{14}$$

and

$$|Q_1| = 3Q^1_{S_\pm}, \quad Q^1_{S_\pm} = -\frac{B}{16C}\left[1 \pm \left[1 - \frac{64AC}{3B^2}\right]^{1/2}\right]. \tag{15}$$

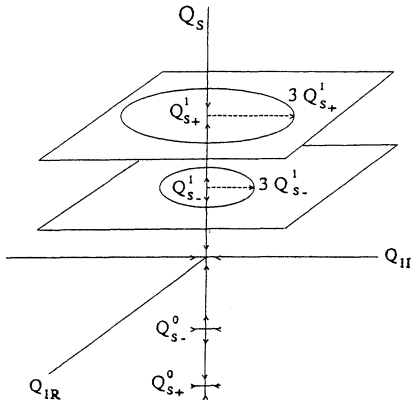

FIG. 2. Fixed points in the space (Q_S, Q_{1R}, Q_{1I}).

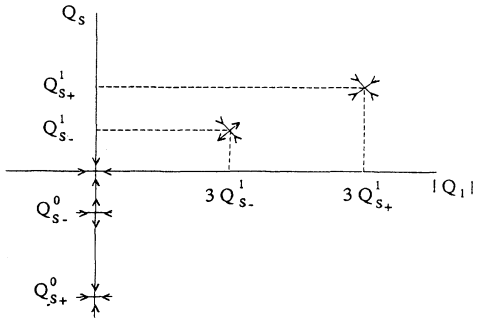

FIG. 3. Fixed points in the space $(Q_S, |Q_1|)$.

The relative stability of each fixed point, as a function of temperature, is given in Appendix B, but in all cases there are only three possible stable fixed points (equilibrium states). The meaning of these stable fixed points is obtained by expressing the three eigenvalues λ_i of the tensor order parameter Q_{ij} as functions of the set of variables (Q_S, Q_1)

$$\lambda_0 = -Q_S, \quad \lambda_\pm = \frac{Q_S}{2} \pm \frac{|Q_1|}{2}. \tag{16}$$

Then the point $(Q_S = Q_1 = 0)$ corresponds to the isotropic state, $(|Q_1| = 0,\ Q_S = Q^0_{S_+})$ to a uniaxial $(\lambda_+ = \lambda_-)$ equilibrium nematic state, and $(|Q_1| = 3Q_S,\ Q_S = Q^1_{S_+})$ to another uniaxial $(\lambda_+ = \lambda_0$ or $\lambda_- = \lambda_0)$ nematic phase. The difference between these two anisotropic states is related to the associated director field. With the help of Eqs. (8), we identify the first nematic state, which corresponds to a homeotropic $(\theta = 0)$ configuration of the director $\hat{n}$ with an orientational order parameter S, which satisfies $S = -Q_S$.

The second mesophase corresponds to an equilibrium state with a homogeneous "degenerated" planar configuration of the director $(\theta = \pi/2)$. The direction always remains in the plane (x,y) during the time evolution, but all the possible orientations in this plane are energetically equivalent (the modulus of Q_1 only is specified, see Fig. 2) and thus allowed. This fact explains the possibility of defect creation in the nematic phase. From Eqs. (8), we verify that the uniaxial order parameter obeys $S = 2Q_S$, the solution when the surfaces impose a degenerate planar anchoring.

D. Isotropic to anisotropic phase transition

The model can describe two types of anchoring: the positive Q_S values concerning the planar degenerate case $(S = 2Q_S)$ and the negative Q_S values concerning the homeotropic case $(S = -Q_S)$ (see the phase portrait, Figs. 2 and 3). As the temperature is abruptly decreased, the initial isotropic equilibrium state becomes metastable with respect to the more stable—homeotropic or planar—nematic phase. Then the first-order phase transition cannot take place unless there are some fluctuations, spatially localized and of sufficiently large amplitude, that constitute the nuclei of the more stable nematic phase and enable the system to overcome the energy bar-

rier [located at the saddle fixed points ($|Q_1|=0$, $Q_S=Q_{S-}^0$) for the homeotropic anchoring and ($|Q_1|=3Q_{S-}^1$, $Q_S=Q_{S-}^1$) for the degenerate planar anchoring, respectively, and where the free energy density is a maximum]. This is a nucleation and growth phenomenon.

Thus the selection of the initial fluctuations, inside the isotropic metastable phase, is the decided starting point for the simulations and must correspond to the physical reality. It depends of the choice of the anchoring, homeotropic or planar degenerate. For a degenerate planar anchoring, the fluctuations must satisfy $Q_1 \neq 0$ and $Q_S > 0$ and then the initial state has a Q_S mean value slightly shifted up from $Q_S=0$; for a homeotropic anchoring, the fluctuations obey $Q_1=0$ and $Q_S<0$ and then the initial state has a Q_S mean value slightly shifted down from $Q_S=0$. Once the initial state has been fixed according to the chosen anchoring, the system evolves towards a determined physical nematic state and the unphysical coexistence between planar and homeotropic states is prohibited.

1. *Homeotropic case*

For a homeotropic uniform director field, the full set of equations is reduced to a single nonlinear equation describing the spatiotemporal evolution of the scalar orientational order parameter Q_S

$$\frac{dQ_S}{dt} = -3\left[2AQ_S - \frac{3B}{2}Q_S^2 + 6CQ_S^3 - \left[1-\frac{2K}{3}\right]\nabla^2 Q_S\right], \tag{17}$$

which can be rewritten, with the help of the relation $Q_S=-S$ and after rescaling time and space,

$$\frac{dS}{dt} = -\left[\frac{\partial f}{\partial S} - \nabla^2 S\right], \tag{18}$$

where f is given by

$$f = AS^2 = \frac{B}{2}S^3 + \frac{3}{2}CS^4 . \tag{19}$$

Equation (18) is a nonlinear partial derivative equation of Landau-Ginzburg type for a nonconservative scalar order parameter.

The system is initially prepared in the isotropic state and quenched at a lower reduced temperature T/T_c at which it becomes metastable, that is, between T^*/T_c and 1, the chosen reduced temperature is $T/T_c=0.88$ when $T^*/T_c=0.863$; see Fig. 1. We start the simulations with an initial state with finite fluctuations, with a mean value shifted slightly towards the positive S values, as previously explained.

In Fig. 4 we show the spatiotemporal evolution of the orientational order parameter S [obtained by numerical simulations of Eq. (18)]. The droplets of the more stable anisotropic phase grow in the metastable isotropic continuum. In addition, we note from the orientational order parameter sections that, as soon as the order parameter value inside the droplets has reached its equilibrium value S_+^0, the isotropic-nematic interfaces move aside without changing the shape of the nuclei. There is no depression zone at the base of the droplets, contrary to other nucleation and growth processes (such as, for example, the phase separation in binary mixtures where there is a mass conservation constraint).

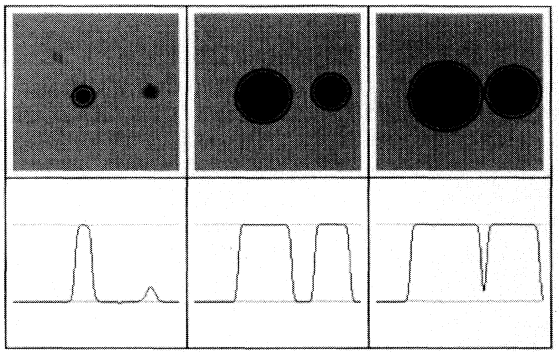

FIG. 4. Time evolution of the orientational order parameter S during the isotropic-homeotropic nematic phase transition (homeotropic anchoring); $T/T_c=0.88$ (see Fig. 3). From left to right: $t/\Delta t=147,270,329$ with time and space units $\Delta t=0.08$ and $\Delta x=1.00$, respectively. Top: two-dimensional gray color visualization (light gray represents the isotropic phase and the dark gray the nematic droplets). Bottom: sections, along x, of the orientational order parameter (the upper horizontal dashed line corresponds to $S=S_+^0$ and the lower one to $S=0$).

By image analysis, we quantitatively study the time evolution of the mean radius of the droplets $R(t)$. It scales (Fig. 5) asymptotically as $R(t) \propto t^{\alpha}$ with $\alpha=1$, which is consistent with the theories of Chan [17], Ostner, Chan, and Kahlweit [18], and Allen and Cahn [19].

When the system is prepared in an anisotropic homogeneous phase and quenched to a higher temperature where the anisotropic phase becomes metastable, that is, between T_c and T^{**} (with $T^{**}/T_c=1.017$), a nucleation and growth process of isotropic droplets takes place with the same time law as for $R(t)$.

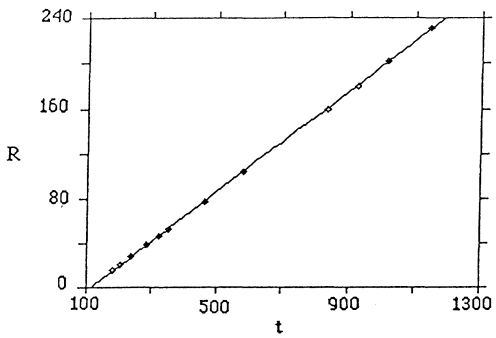

FIG. 5. Time evolution of the droplets mean radius during the phase transition $R(t) \propto t^{\alpha}$ with $\alpha=1$. $R(t)$ and t are dimensionless (length and time have been renormalized $R \rightarrow R/\Delta x$ and $t \rightarrow t/\Delta t$ with $\Delta x=1.2$ and $\Delta t=0.05$).

2. *Planar case*

This is the more interesting case since it allows the description of both the phase transition (nucleation and growth process) and the textures of the planar nematic phase (*Schlieren* textures). This state corresponds to the third set of fixed points and requires the full set of partial derivative equations [Eqs. (9) and (10)].

The calculations are made in the (Q_S, Q_1) plane and the visualization in the physical space, as explained above, by using either a gray field representation or a set of small linear segments describing the local directors (see Fig. 8 as an example). The first representation simulates a crossed polarizers microscope: the dark gray corresponds to an area in which the molecules are parallel either to the analyzer (x axis) or to the polarizer (y axis), while the light gray corresponds to area where the molecules make an angle of 45° both with the analyzer and with the polarizer. Thus the isotopic zones appear either with a black color or with small dots.

We discretize time and space in steps numbers N_t and N_x such that $t=N_t\Delta t$ and $x=N_x\Delta x$, where Δt and Δx are the time and space units. In our simulations, we have used $\Delta t\approx 0.01$ ($K<0$) or $\Delta t\approx 0.05$ ($K>0$) and $\Delta x\approx 1.2$ to ensure good stability of the explicit finite difference scheme.

We initially prepare the system in an isotropic state and quench it to the reduced temperature $T/T_c=0.88$ at which the isotropic state is metastable with respect to the anisotropic phase. As previously explained, we must include, in the initial isotropic state ($Q_S=Q_1=0$), fluctuations of Q_S of sufficiently large amplitude, which shift the mean Q_S value towards a positive value and ensure a bifurcation to the planar anisotropic state (see Fig. 2).

Figure 6 represents the time evolution of the isotropic-anisotropic phase transition, occurring via a nucleation and growth process. The droplets of the stable nematic phase expand to the detriment of the metastable isotropic phase. Then, as any orientations inside the droplets are equiprobable, their coalescence leads to a nematic phase with a lot of topological defects. These defects are of strength $\pm\frac{1}{2}$ and, since the total topological strength must be zero, they recombine by pairs of opposite sign. During the time evolution, pairs of defects annihilate until the system reaches the planar uniform uniaxial phase without any defect, as predicted by the phase portrait.

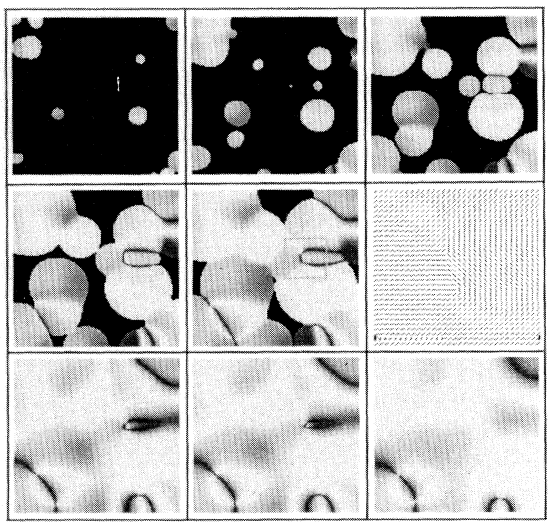

FIG. 6. Time evolution of the director field during the isotropic-nematic phase transition ("degenerate planar" anchoring) at $T/T_c=0.88$, with $K=0$. From left to right and from top to bottom: $t/\Delta t=279,408,577,682,799,799,1304,1439,2613$, with $\Delta t=0.05$ and $\Delta x=1.2$. The configuration, at $t/\Delta t=799$, is visualized with the gray field and the defects $(+\frac{1}{2},-\frac{1}{2})$ (inside the small box) with small linear segments (director field).

We also visualize, in Fig. 7, the three eigenvalues of the tensorial order parameter, in a defect zone, at $T/T_c=0.88$. Starting first with an uniaxial solution of the defect (artificially built), with a thinner isotropic core of nearly one spatial step diameter, we obtain, after relaxation, a defect with a biaxial circular ring around the core (with prolate organization of the molecules) and a uniaxial core (with oblate organization of the molecules) [7]. In the core of the defect, the three eigenvalues are 0.147:0.147:−0.294 and outside the defect zone (homogeneous state) they are 0.99:−0.495:−0495 (uniaxial and prolate medium).

With a more realistic initial condition (nucleation of stable anisotropic zones inside a metastable isotropic continuum), all the defects (such as those shown in Fig. 6) develop with a biaxial core characterized by the three eigenvalues 0.443:−0.115:−0.328. Far from the defect zone, we recover the values of the homogeneous uniaxial state. This behavior is independent of the sign of the half-integral disclination index.

An isolated, artificially built defect cannot escape from the medium and then relax to a pseudoequilibrium state with a uniaxial core. True dynamical defects evolve to a homogeneous phase with a zero global topological strength. So the biaxial structure of these defects corresponds to an out-of-equilibrium configuration of the

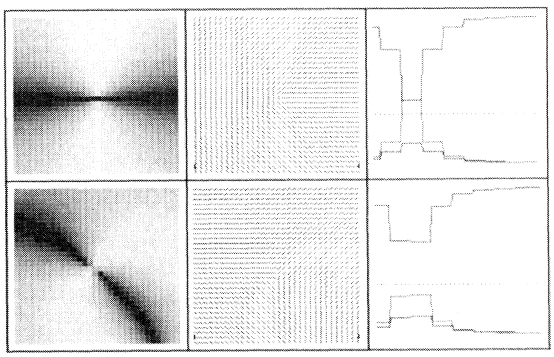

FIG. 7. Three eigenvalues of the tensor order parameter at the core of a defect, at $T/T_c=0.88$ and $K=0$, with $t/\Delta t=0.05$ and $\Delta x=1.2$. Top: defect $(+\frac{1}{2})$ at $t/\Delta t=760$, created from a uniaxial solution at $t=0$. Bottom: Defect $(-\frac{1}{2})$ at $t/\Delta t=2613$, obtained from the isotropic-nematic phase transition (see Fig. 6). The visualizations are made with the gray field (four times magnification), the director field (four times magnification) and sections of the core along the x direction (sixteen times magnifications; the dashed horizontal lines correspond to the zero eigenvalue).

director. Moreover, the radius of the core of the defects increases and the inner biaxiality decreases when the quench temperature becomes closer to the transition temperature.

Finally, we observe that only defects of strength $|s|=\frac{1}{2}$ could appear in our system. This behavior is in agreement with the energetical criterion, derived in the planar model case, with the help of the Frank elastic free energy: the energetic cost of a defect of strength s is proportional to s^2 [20,21]. An escape of a defect of rank 1 in the third dimension, leading to a nonsingular continuous structure, although energetically more favorable, is here prohibited by the anchoring energy. We verify in Fig. 8 that a planar defect of strength 1, arbitrarily built at $t=0$, cannot correspond to a stable configuration and separates into two more energetically favorable defects of strength $+\frac{1}{2}$ (topological charge conservation), which repulse one another during time.

We now briefly study, from a more quantitative point of view, the annihilation laws of an isolate opposite pair of defects of strength $\pm\frac{1}{2}$, in thin nematic films. The simulations are made at various reduced temperatures T/T_c inside the metastability zone of the isotropic phase and then between T^*/T_c and 1. Initially, at $t=0$, the defects are separated by a distance R_0.

In Fig. 9 the time evolution $R(t)$, together with the curve fits, at four reduced temperatures (among the eleven explored ones) is reported. The annihilation occurs more rapidly when the temperature is closer to the transition temperature T_c, where the system is less strongly oriented. Moreover, at a given reduced temperature, the interactions are stronger when the opposite defects are closer to one another. These two simple remarks explain the presence, at low temperature and in the first stages of the time evolution, of a set of points on the curve $R(t)$, having nearly the same ordinate: it is a problem of numerical precision in the location of the defects, due to the very slow evolution of the short time process.

By curve fitting, a time scale law of the form $R(t)\propto(t_0-t)^a$ is obtained, where t_0, the time of defects collapse, is temperature dependent and decreases with increasing temperature (t_0 is calculated with a mean relative error of 2.5×10^{-4}). The exponent a is slightly temperature dependent and varies between 0.337 and 0.355 (with a mean absolute error of 7×10^{-4}), inside the metastability zone. It obeys a law of the form $a\approx\alpha/(\gamma-T/T_c)^{\epsilon}$ with $\alpha\approx0.326\pm0.001$, $\gamma\approx1.007\pm0.001$, and $\epsilon\approx0.018\pm0.001$ (Fig. 10). We note that the parameter γ is slightly different from unity (the value at the transition temperature at which a defect annihilation can always occurs), but never greater than the value of the reduced temperature T^{**}/T_c.

We then obtain a power time scale law $R(t)$ for the de-

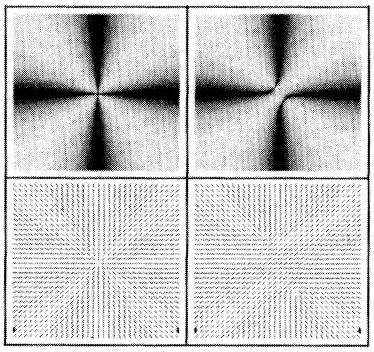

FIG. 8. Separation, at $T/T_c=0.88$ and $K=0$, of a planar defect of strength $+1$ ($t/\Delta t=0$) into two defect s of strength $+\frac{1}{2}$, energetically more favorable (at $t/\Delta t=2819$), with $\Delta t=0.05$ and $\Delta x=1.2$.

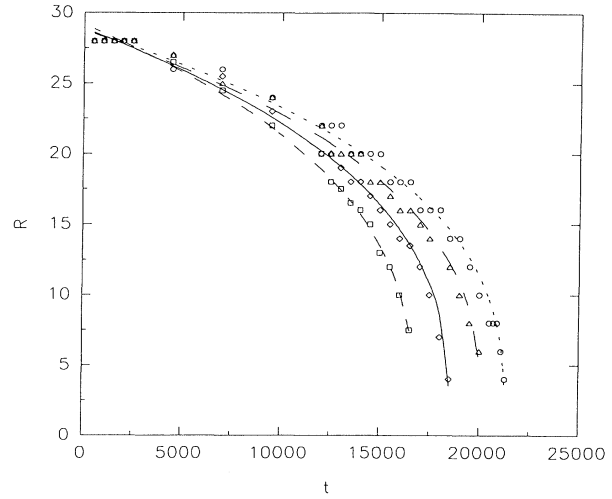

FIG. 9. Time evolution of the distance of separation between two opposite strength defects, isolated in the medium $R(t)\propto(t_0-t)^a$. $R(t)$ and t,t_0 are dimensionless (length and time have been renormalized $R\rightarrow R/\Delta x$ and $t\rightarrow t/\Delta t$ with $\Delta x=1.2$ and $\Delta t=0.05$). □, $T/T_c=0.98$, $a=0.3466$; ◇, $T/T_c=0.95$, $a=0.3422$; △, $T/T_c=0.90$, $a=0.3389$; ∘, $T/T_c=0.866$, $a=0.3371$ (with a mean absolute error on a of 7×10^{-4}).

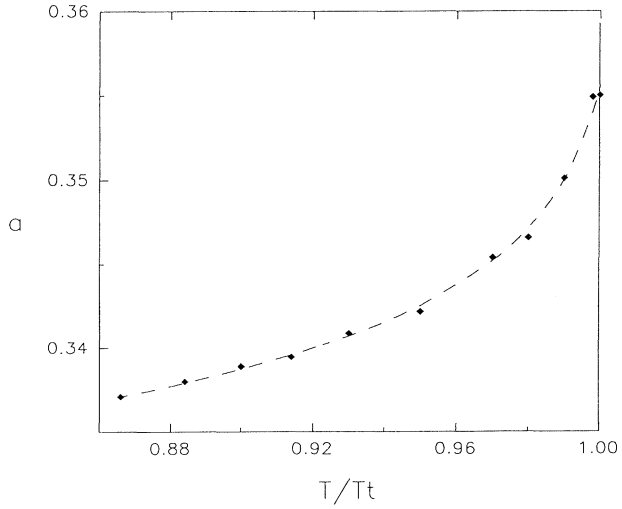

FIG. 10. Reduced temperature dependence of the power exponent a of the $R(t)$ law.

fect annihilation process of the same form as the one derived by de Gennes [4], where the exponent a was temperature independent and equal to $\frac{1}{2}$. In Ref. [4], the interaction force between an opposite pair of defects has been obtained from the nematodynamics equations in which a core energy correction—a cutoff radius being associated with the central defect region—has been taken into account. There the time evolution law of the distance between defects has been derived from hydrodynamics effects (viscous friction force).

On the other hand, our model is purely diffusive and so does not take into account the coupling between fluid flow and orientation (hydrodynamics effects). Furthermore, we consider the corrective contributions, at a given quench temperature, to the free energy related to the continuous variation of the orientational order parameter and to the defect structure: the biaxiality in the neighborhood of the inner core. These reasons help explain the discrepancy between the exponent values in the two approaches.

In real physical experiments, we never obtain a pair of isolated defects of opposite strength. There is instead many defects in the system and the average distance $R(t)$, related to the growing size of monodomains, can be determined via the measurement of the number density of defects $\rho(t)$. The ordering process involves a decrease in $\rho(t)$ and then an increase in the domain size $R(t)$ [22]. The two quantities are obviously interrelated and we have, the case of thin films,

$$R(t) \propto \rho(t)^{-1/2} . \tag{20}$$

$\rho(t)$ is measured either by image analysis [23] or by the evolution of the transmitted light intensity of the sample when the analyzer is removed from the microscope [22,24]. Measurements are moreover realized at intermediate stages, where $\rho(t)$ is sufficiently large [25]. Thus, we determine numerically $\rho(t)$ in order to quantify the influence of the many-body disinclinations interactions (attractive and repulsive ones between different pairs of defects) on the time power law, previously established in a special case.

We prepare the system at high temperature and quench it to a lower one where the isotropic state is metastable with respect to an anisotropic one. As a result of the droplet coalescence phenomenon, it appears that many defects are randomly located in the sample. We calculate the time evolution of the number of defects in the system, at a given reduced temperature ($T/T_c = 0.88$), from ten initial states.

We find the same type of behavior for all the $\rho(t)$ curves. Only the values of the particular time when a drastic change of behavior occurs are different from one run to another one, because of the different initial states.

We nevertheless display two main behaviors corresponding to the early (interaction between a great number of defects pairs) and intermediate (interaction between the two or three nearest pairs of defects) stages of the annihilation process. The very last stage, corresponding to punctual annihilations of isolated pairs of defects, is not significant.

We fit the first two parts of the curves and we find power laws of the form $\rho(t) \propto t^{-b}$ with average exponents, over the ten runs, equal to ≈ 0.1 in the early stages and ≈ 1.1 (with a dispersion lying between 0.7 and 1.5) in the intermediate stages. Experimentally, few authors have shown behaviors of the same t^{-b} form, with an exponent b varying between 0.7 and 1 [22,24,26,27,23]. Our result then, although slightly higher, is in rather good agreement with these experiments. Unfortunately, the dispersion on the individual exponent values is too large to allow the study of the effect of temperature.

We can, however, say that this dependence is very weak. So we obtain [from Eq. (20), at a given temperature] an average growth size of the monodomains $R(t) \propto t^{0.55}$, in the metastability zone. The result, compared with the direct determination of $R(t)$, indicates that the many-body interactions increase rather significantly the exponent of the annihilation time power law.

3. *Effect of the anisotropic elastic term on the isotropic to anisotropic phase transition and interfaces, in the planar case*

We have previously seen, in the planar degenerate anchoring case, with $K=0$, that the isotropic-anisotropic phase transition takes place via the nucleation of spatially isotropic domains of the stable nematic phase into a continuum of the metastable isotropic phase. The introduction of the anisotropic elastic term $K \neq 0$ leads to a spatially anisotropic growth of the nematic droplet. In the Landau free energy expression, expanded to the second order in the gradient terms [Eq. (2), in the uniaxial limit and with any uniform direction $\hat{\mathbf{n}}$], the two spatial derivative terms are proportional, respectively, to $(L_1+L_2/6)(\nabla S)^2$, which is spatially isotropic, and $(L_2/2)(\hat{\mathbf{n}}\cdot\nabla S)^2$, which is the spatially anisotropic term. Once the director has been chosen, for example, along the x axis, we have two terms of the form $(L_1+2/3L_2)(\partial_x S)^2$ and $(L_1+L_2/6)(\partial_y S)^2$. These spatial derivative contributions to the free energy density lead to two diffusion terms $(L_1+2/3L_2)\partial_x^2 S$ and $(L_1+L_2/6)\partial_y^2$, into the spatiotemporal evolution equations (9) and (10). Then, if $K>0$ ($K<0$), which means $L_2>0$ ($L_2<0$), the diffusion coefficient along the x direction, the chosen director direction, is more (less) important than the diffusion coefficient along the y direction and so the droplet increases more rapidly in the x (y) direction, which is parallel (perpendicular) to the director.

Since the system of spatiotemporal equations is rotationally invariant, the preceding qualitative reasoning is true whatever the chosen orientation of the uniform director inside the domain: when $K>0$, the domain grows preferentially along the director and when $K<0$, it grows preferentially perpendicular to the director. Such anisotropic growth of domains are shown numerically in Fig. 11, for a positive (physical case) and a negative K value, with an initial uniform director chosen along the x axis.

We now study the spatiotemporal development of the interface. In the case $K=0$ (Fig. 12, first row), a spatially

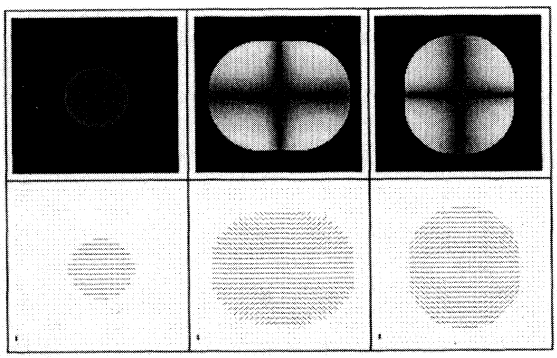

FIG. 11. Effect of the (dimensionless) anisotropic elasticity term K on the shape of a growing nematic droplet, with a uniform director (parallel to the x axis), inside a metastable phase, at $T/T_c=0.88$. From left to right: $K=0$, $t/\Delta t=537$ (with $\Delta t=0.05$); $K=0.4$, $t/\Delta t=1097$ (with $\Delta t=0.05$); and $K=-0.4$, $t/\Delta t=4993$ (with $\Delta t=0.01$). Upper and lower rows: gray and director field representations.

isotropic droplet (initially prepared with a uniaxial planar configuration) develops with time with a biaxial interface, the biaxiality being invariant with respect to droplet rotation.

The effect of a nonzero elasticity anisotropy term $K>0$ is to induce, transiently, a spatially anisotropic character of the interface biaxiality, in the intermediate stage of the spatiotemporal evolution. Indeed, as seen in Fig. 12, for $K>0$ and a uniform director along the x axis, the interface is biaxial in the main x direction of growth (Fig. 12, second row), where the local directors lie perpendicular to it, while it remains uniaxial (or very poorly biaxial) in the orthogonal direction (Fig. 12, third row).

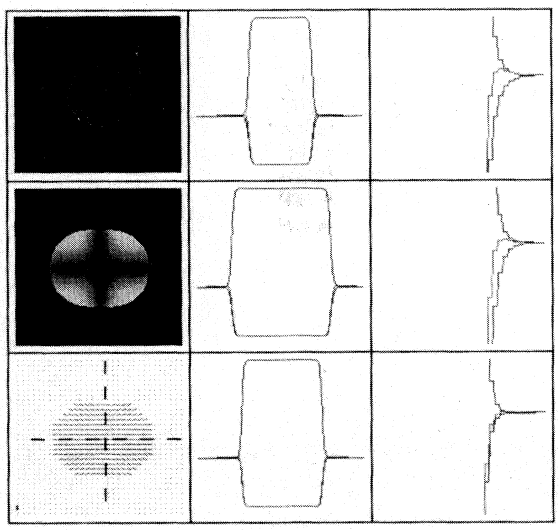

FIG. 12. Biaxiality at the isotropic-nematic interface, at $T/T_c=0.88$, with $\Delta t=0.05$ and $\Delta x=1.2$. Top: $K=0$, $t/\Delta t=537$. From left to right: two-dimensional gray field visualization and section along the x axis (rotationally invariant) showing the three eigenvalues and four times magnification of the section, at the interface. Middle and bottom: $K=0.4$, $t/\Delta t=772$. From left to right: a two-dimensional gray field and the corresponding director field (where the two directions of section are shown); the three eigenvalues along the x (middle) and y (bottom) axes and four times magnification of these sections at the interface.

Later on, due to the nonlinear terms in the evolution equations set, defects appear inside the droplet (Fig. 13). Indeed, as a result of the different growth rates, depending on whether the local directors are parallel or perpendicular to the interface, the interface suffers deformations leading to the emergence of dips in the y direction and the creation of a pair of defects $+\frac{1}{2}$, along the same axis, inside the domain. The local director is again perpendicular to the interface in the bottom of the wells and the dips fill in; then the isotropic-anisotropic interface recovers its biaxial character at any points. These behaviors have been verified with any uniform orientation inside the uniaxial nematic droplet.

However, the stage where defects appear inside the droplet is prevented, in real nematic samples, by the formation of many droplets whose growth is generally stopped by the coalescence phenomena between neighbors leading to defect creation. The biaxial character of the droplet interface explains why the core of the defects itself also has a biaxial structure.

Finally, we note that the presence of the anisotropic term K (which leads to coupling between the spatial variations of the directors and of the orientational order parameters) does not significantly modify the time laws of pair annihilation previously obtained. For a thin, uniaxial, nematic film, only the bend and splay elastic constants play a role in the sample deformation. Then, since the present model imposes, at the considered expansion order, equal bend and splay constants, there is no anisotropic effect to the relative spatial positions of two defects of opposite strength nor different evolution laws for the $+\frac{1}{2}$ and $-\frac{1}{2}$ strength defects [20,21,28,29].

E. Anisotropic to isotropic phase transition

The degenerated planar anisotropic state containing some defects can become metastable with respect to the isotropic phase when the reduced temperature is between 1 and T^{**}/T_c. Then, as in the case of the isotropic-anisotropic phase transition, a nucleation and growth process takes place. The cores of the defects of the anisotropic phase, which are not isotropic but rather correspond to lower values of Q_S (located around the saddle

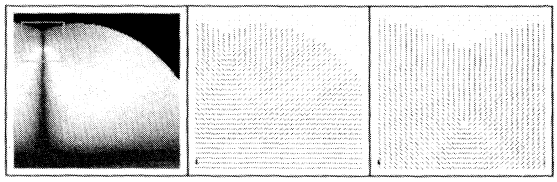

FIG. 13. Late stages of the spatiotemporal evolutions of a droplet, with an initial uniform orientation of the director (along the x direction), at $T/T_c=0.88$ and $K=0.4$ (see Fig. 12); $t/\Delta t=2299$ with $\Delta t=0.05$ and $\Delta x=1.2$. From left to right: gray field, the corresponding director field, and a zoom of the director field inside the small box.

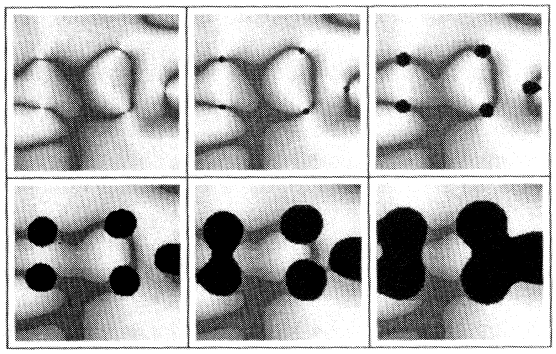

FIG. 14. Start of the anisotropic-isotropic phase transition at the cores of defects, $T/T_c=1.01$ and $K=0$. From left to right and from top to bottom: $t/\Delta t=0.391,975,2008,2640,3114$, with $\Delta t=0.05$ and $\Delta x=1.2$.

fixed point Q_S^1 of the phase portrait), play the role of the initial fluctuations simulating the nuclei of the planar nematic phase inside the metastable isotropic phase (see Sec. III D), which enable the nucleation and growth phenomena to start (it is the amount of energy necessary to render unstable the anisotropic metastable state). Then, the isotropic nucleation naturally takes place in the core of the anisotropic metastable defects, as observed in Fig. 14. These droplets increase in size and coalesce until the system reaches a homogeneous isotropic stable state. This behavior is experimentally observed (Fig. 15) on a thin nematic film of PAA, quenched at a temperature where the anisotropic phase is metastable. Obviously, if the simulations are made at a reduced temperature above T^{**}/T_c, the anisotropic phase becomes unstable and almost the whole sample (and not only the core zones) reaches, nearly instantaneously, an isotropic state.

FIG. 15. Experimental view of the isotropic nucleation at the cores of defects in a semithin film of para azoxyanisole, at a temperature slightly above $T_c=136\,^{\circ}\mathrm{C}$.

1. Effect of the anisotropic elastic term K

This problem is, in all points, equivalent to the growth of a uniformly oriented droplet in an isotropic medium. We know that a uniform nematic domain preferentially grows parallel to the direction of the director when $K>0$ and perpendicularly to it when $K<0$. The same behavior is recovered when we study the growth of an isotropic droplet in a uniform nematic medium. Figure 16 shows the numerical simulations of the isotropic droplet growth in the cores of an opposite pair of defects $(+\frac{1}{2}, -\frac{1}{2})$ for a physical, positive K value ($K\approx 0.4$).

We can qualitatively explain the anisotropic shape of the isotropic droplets by separating the director field around the defect core into several anisotropic zones, with an early uniform director. As K is positive, the zones of the isotropic phase grow more quickly when the surrounding nematic director is perpendicular to their interfaces than when the director is parallel to them. So the isotropic zones are elongated along the surrounding nematic director (see Fig. 17, gray schematic ellipses in which the previous orientation of the director is shown). Then we superimpose these anisotropic areas to build the real spatially anisotropic shape (Fig. 17, the external dotted line) of the isotropic phase domain. We have seen that the cores of the defects constitute the germs of the isotropic nucleation; thus we explain the anisotropic shapes of the droplets observed in our numerical simulations with this qualitative argument and in particular the more pronounced anisotropic shape for the isotropic phase domains in the core of the $-\frac{1}{2}$ defects than in the core of the $+\frac{1}{2}$ defects. This last observation is due to the fact that $+\frac{1}{2}$ defects mainly imply bend deformations and $-\frac{1}{2}$ ones splay deformations. Contrary to anisotropic nucleation, we do not observe any significative biaxial interfacial zone. When $K<0$, the droplets grow preferentially perpendicularly to the director and it is easy to make the same qualitative reasoning on the schematic representations of the defects in order to build the resultant domains. Then we have for each defect the same, but reversed (mirror image), shapes as in the case $K>0$.

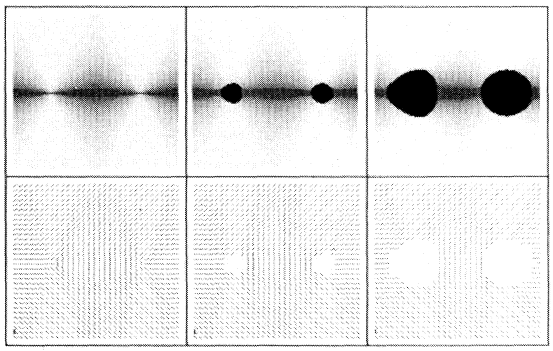

FIG. 16. Numerical simulations of the shape of the nucleating isotropic domains, at $T/T_c=1.01$ and $K=0.4$. From left to right: $t/\Delta t=0,1515,3322$, with $\Delta t=0.05$ and $\Delta x1.2$. Top: gray colors. Bottom: director fields.

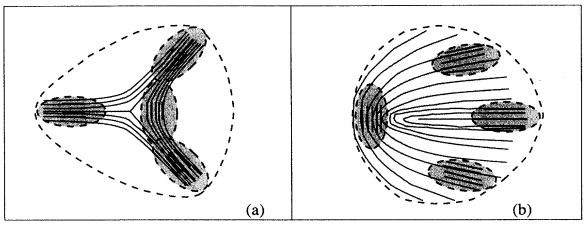

FIG. 17. Schematic representation of the shape of the nucleating isotropic domains (dotted line), from the core of defects of strength $+\frac{1}{2}$ and $-\frac{1}{2}$, with $K>0$, as obtained from the superposition of elongated (along the nearly uniform surrounding director) isotropic zones (gray ellipses).

IV. CONCLUSION

In this work, we have reproduced the main behaviors of a thermotropic nematic thin film with the help of a phenomenological Ginzburg-Landau approach. We have taken into account both the orientational order parameters and the directors of the system. With this approach, we have described the isotropic-anisotropic phase transition, with particular emphasis on the nematic defects (annihilation laws) and the biaxiality zones.

In addition, we have analytically and numerically observed a nucleation and growth phenomenon of anisotropic droplets, when an anisotropic elasticity parameter K has been taken into account. This growth occurs, preferentially, along the direction of the director when $K>0$ (the physical situation where the twist elastic constant is lower than the splay and bend constants) and perpendicularly to it when $K<0$.

Finally, we have shown that, when the anisotropic nematic phase becomes metastable, the isotropic nucleation takes place in the core of the defects. The role of germs of nucleation played by the defects core has been confirmed experimentally in a thin nematic film of PAA.

In addition we note that, when an anisotropic elasticity term is included in the equations, the shape of the domain of the isotropic phase becomes anisotropic and is different according to the sign of the topological charge of the defects. This behavior could be experimentally analyzed with the help of a polarizing microscope coupled with an image analysis system, on thin nematic films.

We must note that our model is purely diffusive. So the important effects related to the coupling between the director motion and the fluid flow are not taken into account. Thus we plan to introduce in a future paper the hydrodynamic equations of motion of a liquid crystal [30–32] in order to see the modifications of the domains shape during the isotropic nucleation and the corrections to the annihilation law of an opposite strength defect pair.

From a theoretical point of view, the model can be extended to the study of the influence of a strong quadratic [16] or linear anchoring [33] or of an external field (magnetic, electric or elongational) [34] on the nature of the phase transition (biaxial states, quasi-two-dimensional second-order transition) and on the defects behaviors (for example, Lehmann clusters [35]). In addition, the full model (with spatial variations of the director along the z axis) can be used to describe more complex problems such as the phase transition and defects behaviors in thin nematic films sandwiched between two different isotropic media (confined geometry) [36].

ACKNOWLEDGMENT

We thank the Conseil Régional Provence-Alpes-Côte d'Azur for financial support in order to use the computers of the Centre Régional de Calcul et Télécommunication Scientifique and INRIA Sophia-Antipolis where the calculations have been performed.

APPENDIX A

The set of coupled nonlinear partial derivatives describing the spatiotemporal evolutions of the components of the tensorial order parameter is written, after the changes of variables and rescaling (where we have replaced $\bar{t}$ and $\bar{x}$, respectively, by t and x in order to simplify the notation) explicitly described in Sec. II C

$$\frac{\partial Q_S}{\partial t}=-3\left\{\frac{B}{4}(2|Q_1|^2-|Q_2|^2)+\left[2A-\frac{3B}{2}Q_S+2C(3Q_S^2+|Q_1|^2+|Q_2|^2)\right]Q_S-\left[1-\frac{2}{3}K\right]\nabla^2 Q_S\right.$$

$$\left.-\frac{K}{2}(\partial_1^2 Q_{1R}-\partial_2^2 Q_{1R}+3\partial_3^2 Q_S+2\partial_1\partial_2 Q_{1I}-\partial_1\partial_3 Q_{2R}-\partial_2\partial_3 Q_{2I})\right\},$$

$$\frac{\partial Q_{1R}}{\partial t}=-\left\{\frac{3B}{4}(Q_{2R}^2-Q_{2I}^2)+[2A+3BQ_S+2C(3Q_S^2+|Q_1|^2+|Q_2|^2)]Q_{1R}-\nabla^2 Q_{1R}\right.$$

$$\left.-K[\partial_1^2 Q_S-\partial_2^2 Q_S-\partial_3^2 Q_{1R}+\partial_1\partial_3 Q_{2R}-\partial_2\partial_3 Q_{2I}]\right\},$$

$$\frac{\partial Q_{1I}}{\partial t}=-\left\{\frac{3B}{4}(2Q_{2R}Q_{2I})+[2A+3BQ_S+2C(3Q_S^2+|Q_1|^2+|Q_2|^2)]Q_{1I}-\nabla^2 Q_{1I}\right.$$
$$\left.-K[2\partial_1\partial_2 Q_S-\partial_3^2 Q_{1I}+\partial_1\partial_3 Q_{2I}-\partial_2\partial_3 Q_{2R}]\right\},$$
$$\frac{\partial Q_{2R}}{\partial t}=-\left\{\frac{3B}{4}(2Q_{1I}Q_{2I})+\left[2A+\frac{3B}{2}(Q_{1R}-Q_S)+2C(3Q_S^2+|Q_1|^2+|Q_2|^2)\right]Q_{2R}-\nabla^2 Q_{2R}\right.$$
$$\left.-K[-\partial_1\partial_3 Q_S-\partial_2^2 Q_{2R}+\partial_1\partial_2 Q_{2I}+\partial_2\partial_3 Q_{1I}+\partial_1\partial_3 Q_{1R}]\right\},$$
$$\frac{\partial Q_{2I}}{\partial t}=-\left\{\frac{3B}{4}(2Q_{1I}Q_{2R})+\left[2A-\frac{3B}{2}(Q_{1R}+Q_S)+2C(3Q_S^2+|Q_1|^2+|Q_2|^2)\right]Q_{2I}-\nabla^2 Q_{2I}\right.$$
$$\left.-K[-\partial_2\partial_3 Q_S-\partial_1^2 Q_{2I}+\partial_1\partial_2 Q_{2R}-\partial_2\partial_3 Q_{1R}+\partial_1\partial_3 Q_{1I}]\right\}.$$

APPENDIX B

We study the stability of the fixed points defined in Sec. III C with respect to infinitesimal fluctuations δQ_S, δQ_{1R}, and δQ_{1I}. Then the stability matrix is obtained by linearizing the system of equations, and the sign of its eigenvalues allows the determination of the type of stability in the same way that the local curvature is determined in the case of a one-dimensional curve.

We find that the first fixed point [Eq. (13)] is stable for $T>T^*$ and unstable for $T<T^*$. For the second set of fixed points [Eqs. (14), ($Q_1=0$, $Q_S=Q_{S_+}^0$) is always stable for $T<T^{**}$ and ($Q_1=0$, $Q_S=Q_{S_-}^0$) is a saddle point. In this last case, we note that it is an attractive fixed point along Q_{1R} and Q_{1I} (Q_S) and a repulsive one along Q_S (Q_{1R} and Q_{1I}) for $T^*<T<T^{**}$ ($T<T^*$) (see Figs. 1 and 2). For the last set of fixed points, ($|Q_1|=3Q_S, Q_S=Q_{S_+}^1$) is stable for all temperatures lower than T^{**} and ($|Q_1|=3Q_S$, $Q_S=Q_{S_-}^1$) is always a saddle point in the same range of temperatures.

To fix ideas on the stability of the fixed points studied above, we develop the case of the homeotropic liquid crystal in which the fixed points under consideration are on a simple curve drawn on a hypersurface (Q_{1R}, Q_{1I}, Q_S). The free energy density is written here as

$$f\propto AQ_S^2-\frac{B}{2}Q_S^3+\frac{3C}{2}Q_S^4, \tag{B1}$$

with $Q_S=-S$ [see Eq. (8)], where S is the uniaxial orientational order parameter (degree of order of the molecules around the fixed uniform direction $\hat{\mathbf{n}}=n_z\hat{z}$).

In Fig. 1 we represent the shape of the preceding free energy density in which we have made the substitution $Q_S\rightarrow -S$ as a function of the temperature. Then, we verify that $S=S_-^0$ is unstable (the free energy curvature is negative), $S=S_+^0$ is stable (positive curvature), and so the isotropic state $S=0$ is stable. In fact, the isotropic state is stable until T reaches T_c and metastable between T_c and T^*, the anisotropic state S_+^0 is stable below T_c and metastable between T_c and T^{**}, but our perturbational theory (infinitesimal fluctuations) cannot take into account this type of stability (the fluctuations must be sufficiently large in amplitude to render unstable a metastable state).

Finally, we note that at equilibrium, the planar case corresponds to $Q_S=S/2$ [see Eq. (8) with $\theta=\pi/2$] and that, as B is a negative temperature-dependent coefficient, the orientational order parameter is positive in all the equilibrium configurations. This is not always the case when an external field (magnetic, electric, or elongational) is applied to the sample [34].

[1] S. Chandrasekhar, *Liquid Crystals* (Cambridge University Press, Cambridge, 1992).
[2] J. D. Gunton, M. San Miguel, and P. S. Sahni, in *Phase Transitions and Critical Phenomena,* edited by C. Domb and J. L. Lebowitz (Academic, New York, 1983), Vol. 8.
[3] P. G. de Gennes, Mol. Cryst. Liq. Cryst. **12**, 193 (1971).
[4] P. G. de Gennes, *The Physics of Liquid Crystal* (Clarendon, Oxford, 1974).
[5] A. Killian, Mol. Cryst. Liq. Cryst. **222**, 57 (1992).
[6] H. Mori, Prog. Theor. Phys. **33**, 423 (1965); S. K. Ma and G. Mazenko, Phys. Rev. B **11**, 4077 (1975).
[7] N. Schopohl and T. J. Slukin, Phys. Rev. Lett. **59**, 2582 (1987).
[8] Ping Sheng, in *Introduction to Liquid Crystals,* edited by E. B. Priestley, P. J. Wojtowicz, and Ping Sheng (Plenum, New York, 1979).
[9] Y. Lansac and P. Maïssa, Physica A **180**, 53 (1992).
[10] F. C. Frank, Discuss. Faraday Soc. **25**, 19 (1958).
[11] F. Leenhouts, H. J. Roebers, A. J. Dekker, and J. J. Jonker, J. Phys. (Paris) Colloq. **40**, C3-291 (1979).

[12] J. D. Bunning, T. E. Faber, and P. L. Sherrell, J. Phys. (Paris) **42**, 1175 (1981).
[13] M. J. Stephen and J. P. Straley, Rev. Mod. Phys. **46**, 617 (1974).
[14] H. Gruler, Z. Naturforsch. Teil A **30**, 230 (1975).
[15] H. Metiu, K. Kitahara, and J. Ross, in *Fluctuation Phenomena,* edited by E. W. Montroll and J. L. Lebowitz (Elsevier, New York, 1979), Chap. 4.
[16] R. M. Hornreich, E. I. Kats, and V. V. Lebedev, Phys. Rev. A **46**, 4935 (1992).
[17] S. K. Chan, J. Chem. Phys. **67**, 5755 (1977).
[18] W. Ostner, S. K. Chan, and M. Kahlweit, Ber. Bunsenges. **77**, 1122 (1973).
[19] S. M. Allen and J. W. Cahn, Acta Metall. **27**, 1017 (1979); **27**, 1085 (1979).
[20] S. Chandrasekhar, Adv. Phys. **35**, 507 (1986).
[21] M. Kléman, Rep. Prog. Phys. **52**, 555 (1989).
[22] T. Shiwaku, A. Nakai, H. Hasegawa, and T. Hashimoto, Macromolecules **23**, 1590 (1990).
[23] I. Chuang, N. Turok, and B. Yurke, Phys. Rev. Lett. **66**, 2472 (1991).
[24] T. Shiwaku, A. Nakai, H. Hasegawa, and T. Hashimoto, Polym. Commun. **28**, 175 (1987).
[25] J. Rieger, Macromolecules **23**, 1545 (1990).
[26] H. Orihara, J. Phys. Soc. Jpn. **55**, 2151 (1986).
[27] T. Nagaya, H. Orihara, and Y. Ishibashi, J. Phys. Soc. Jpn. **56**, 3086 (1987).
[28] I. Pardowitz and S. Hess, J. Chem. Phys. **76**, 1485 (1982).
[29] L. Longa, Mol. Cryst. Liq. Cryst. **191**, 49 (1990).
[30] J. L. Ericksen, Arch. Ration. Mech. Anal. **4**, 231 (1960); Phys. Fluids **9**, 1205 (1966).
[31] F. M. Leslie, Q. J. Mech. Appl. Math. **19**, 357 (1966); Arch. Ration. Mech. Anal. **28**, 265 (1968).
[32] O. J. Parodi, J. Phys. (Paris) **31**, 581 (1970).
[33] Y. L'vov, R. M. Hornreich, and D. W. Allender, Phys. Rev. E **48**, 1115 (1993).
[34] P. Palffy-Muhoray and D. A. Dunmur, Mol. Cryst. Liq. Cryst. **97**, 337 (1983).
[35] S. D. Hudson and E. L. Thomas, Phys. Rev. A **44**, 8128 (1991).
[36] O. D. Lavrentovitch, Phys. Scr. **T39**, 394 (1991).

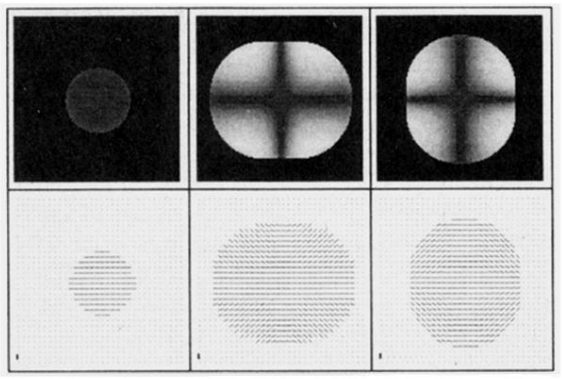

FIG. 11. Effect of the (dimensionless) anisotropic elasticity term K on the shape of a growing nematic droplet, with a uniform director (parallel to the x axis), inside a metastable phase, at $T/T_c=0.88$. From left to right: $K=0$, $t/\Delta t=537$ (with $\Delta t=0.05$); $K=0.4$, $t/\Delta t=1097$ (with $\Delta t=0.05$); and $K=-0.4$, $t/\Delta t=4993$ (with $\Delta t=0.01$). Upper and lower rows: gray and director field representations.

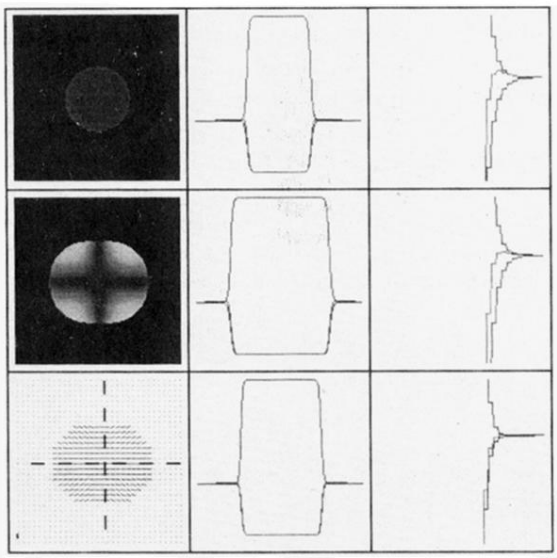

FIG. 12. Biaxiality at the isotropic-nematic interface, at $T/T_c=0.88$, with $\Delta t=0.05$ and $\Delta x=1.2$. Top: $K=0$, $t/\Delta t=537$. From left to right: two-dimensional gray field visualization and section along the x axis (rotationally invariant) showing the three eigenvalues and four times magnification of the section, at the interface. Middle and bottom: $K=0.4$, $t/\Delta t=772$. From left to right: a two-dimensional gray field and the corresponding director field (where the two directions of section are shown); the three eigenvalues along the x (middle) and y (bottom) axes and four times magnification of these sections at the interface.

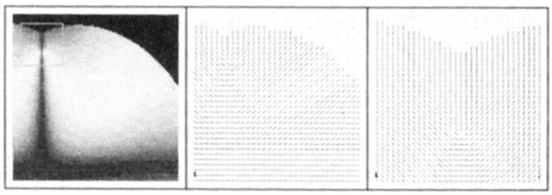

FIG. 13. Late stages of the spatiotemporal evolutions of a droplet, with an initial uniform orientation of the director (along the x direction), at $T/T_c=0.88$ and $K=0.4$ (see Fig. 12); $t/\Delta t=2299$ with $\Delta t=0.05$ and $\Delta x=1.2$. From left to right: gray field, the corresponding director field, and a zoom of the director field inside the small box.

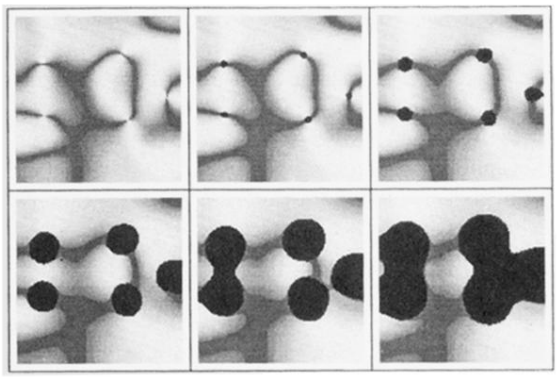

FIG. 14. Start of the anisotropic-isotropic phase transition at the cores of defects, $T/T_c = 1.01$ and $K = 0$. From left to right and from top to bottom: $t/\Delta t = 0.391,975,2008,2640,3114$, with $\Delta t = 0.05$ and $\Delta x = 1.2$.

FIG. 15. Experimental view of the isotropic nucleation at the cores of defects in a semithin film of para azoxyanisole, at a temperature slightly above $T_c = 136\,°C$.

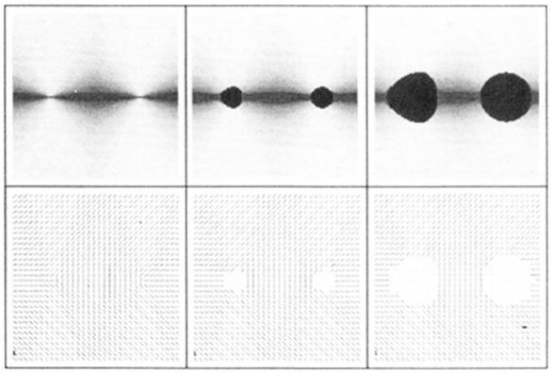

FIG. 16. Numerical simulations of the shape of the nucleating isotropic domains, at $T/T_c = 1.01$ and $K = 0.4$. From left to right: $t/\Delta t = 0,1515,3322$, with $\Delta t = 0.05$ and $\Delta x 1.2$. Top: gray colors. Bottom: director fields.

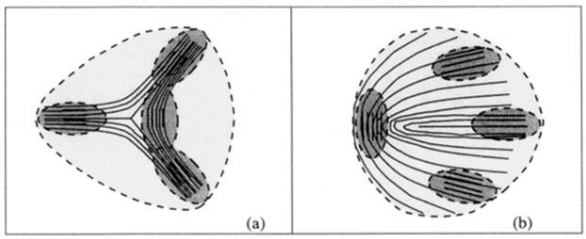

FIG. 17. Schematic representation of the shape of the nucleating isotropic domains (dotted line), from the core of defects of strength $+\frac{1}{2}$ and $-\frac{1}{2}$, with $K > 0$, as obtained from the superposition of elongated (along the nearly uniform surrounding director) isotropic zones (gray ellipses).

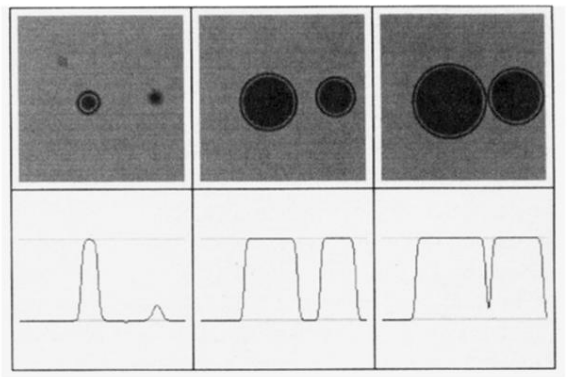

FIG. 4. Time evolution of the orientational order parameter S during the isotropic-homeotropic nematic phase transition (homeotropic anchoring); $T/T_c = 0.88$ (see Fig. 3). From left to right: $t/\Delta t = 147,270,329$ with time and space units $\Delta t = 0.08$ and $\Delta x = 1.00$, respectively. Top: two-dimensional gray color visualization (light gray represents the isotropic phase and the dark gray the nematic droplets). Bottom: sections, along x, of the orientational order parameter (the upper horizontal dashed line corresponds to $S = S_+^0$ and the lower one to $S = 0$).

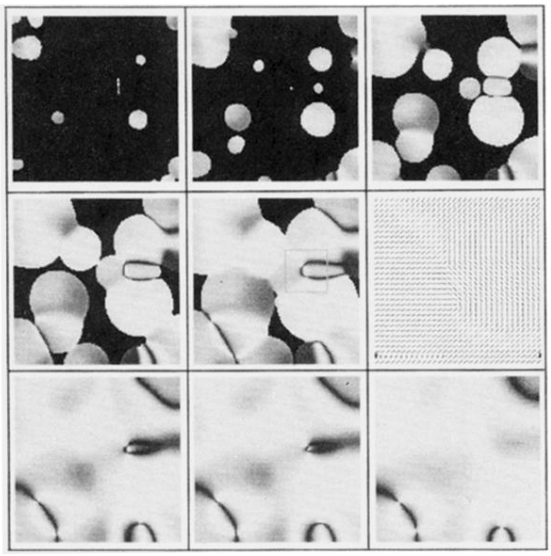

FIG. 6. Time evolution of the director field during the isotropic-nematic phase transition ("degenerate planar" anchoring) at $T/T_c = 0.88$, with $K = 0$. From left to right and from top to bottom: $t/\Delta t = 279,408,577,682,799,799,1304,1439,2613$, with $\Delta t = 0.05$ and $\Delta x = 1.2$. The configuration, at $t/\Delta t = 799$, is visualized with the gray field and the defects $(+\frac{1}{2}, -\frac{1}{2})$ (inside the small box) with small linear segments (director field).

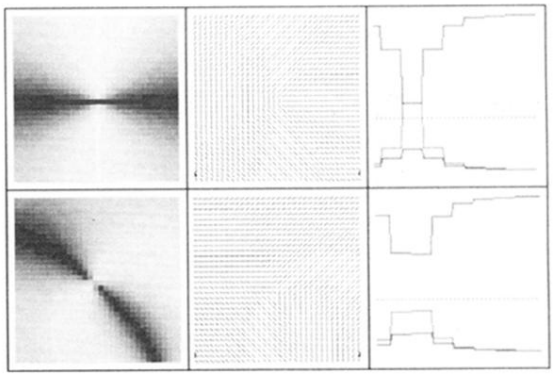

FIG. 7. Three eigenvalues of the tensor order parameter at the core of a defect, at $T/T_c=0.88$ and $K=0$, with $t/\Delta t=0.05$ and $\Delta x=1.2$. Top: defect $(+\frac{1}{2})$ at $t/\Delta t=760$, created from a uniaxial solution at $t=0$. Bottom: Defect $(-\frac{1}{2})$ at $t/\Delta t=2613$, obtained from the isotropic-nematic phase transition (see Fig. 6). The visualizations are made with the gray field (four times magnification), the director field (four times magnification) and sections of the core along the x direction (sixteen times magnifications; the dashed horizontal lines correspond to the zero eigenvalue).

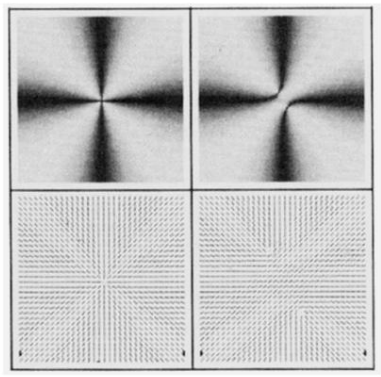

FIG. 8. Separation, at $T/T_c = 0.88$ and $K = 0$, of a planar defect of strength $+1$ ($t/\Delta t = 0$) into two defect s of strength $+\frac{1}{2}$, energetically more favorable (at $t/\Delta t = 2819$), with $\Delta t = 0.05$ and $\Delta x = 1.2$.